Increased receptor binding capability of the SARS-CoV-2 saltational variant PJ.2.1

PeiZhuo He[1,2,#], BingKun Li[1,2,#], Caiwan Guo[1,4], Lingling Yu[1], Yuanling Yu[1], Fanchong Jian[3], Fei Shao[1], Yunlong Cao[1,3,5,*]

[1]Changping Laboratory, Beijing, P. R. China.

[2]Chinese Academy of Medical Sciences & Peking Union Medical College.

[3]Biomedical Pioneering Innovation Center (BIOPIC), School of Life Sciences, Peking University, Beijing, P. R. China.

[4]Academy for Advanced Interdisciplinary Studies, Peking University, Beijing, P. R. China.

[5]Peking–Tsinghua Center for Life Sciences, Peking University, Beijing, P.R. China.

[*]Correspondence: Yunlong Cao (yunlongcao@pku.edu.cn).

[#]These authors contributed equally.

Abstract

The recently identified SARS-CoV-2 saltational variant PJ.2.1, a highly mutated descendant of MC.10.1, has achieved rapid intercontinental spread since its detection in May 2026. Here, we show that PJ.2.1 exhibits exceptionally high human ACE2-binding capability, significantly outperforming contemporary variants such as NB.1.8.1, XFG, and BA.3.2.2. However, despite acquiring over 25 spike mutations, PJ.2.1 remains antigenically similar to the circulating JN.1 family and does not display strong humoral immune evasion. Neutralization profiling indicates that PJ.2.1 possesses heightened neutralization sensitivity to human plasma and RBD-targeting antibodies, especially against cryptic-site-targeting class 4 and class 5 antibodies. This distinct sensitivity profile strongly suggests an altered spike structural dynamic that favors a receptor-accessible "up" conformation. While PJ.2.1 currently lacks the extreme immune evasion capabilities of other contemporary strains, its robust baseline receptor binding strength mirrors the early evolutionary trajectory of BA.2.86 to JN.1. This high receptor binding affinity provides a structural buffer that could facilitate the rapid acquisition of potent immune-evasive mutations, necessitating continued genomic, epidemiological, and virological surveillance of PJ.2.1.

Results

The emergence of saltational SARS-CoV-2 variants, such as BA.1 and BA.2.86, has historically enhanced immune evasion, repeatedly reshaped the pandemic landscape, and prompted critical updates to vaccine formulations [1-2]. As a highly mutated saltational descendant of MC.10.1, the recently discovered PJ.2.1 has acquired more than 25 spike mutations and achieved intercontinental spread. This raises global concerns regarding its potential to alter the SARS-CoV-2 epidemiological trajectory and impact future vaccine strain selection (Figure 1A). These factors warrant immediate investigation into the virological impact of the spike mutations on PJ.2.1.

The first PJ.2.1 sequence was detected in Ontario, Canada, in May 2026. Subsequent wastewater surveillance identified the variant in four New York City sewersheds and one in Utah. Clinical cases quickly emerged in June 2026, followed by international reports from the UK, Spain, and Singapore, underscoring its rapid geographic spread (Figure 1B). Analysis of sequences deposited in the GISAID EpiCoV database revealed two distinct PJ.2.1 lineages that diverge primarily based on N-terminal domain (NTD) mutations. We designated these as PJ.2.1_ON (Ontario) and PJ.2.1_NY (New York) (Figure 1A). Because PJ.2.1_ON was identified earlier and shares key sequence characteristics with the clinical cases reported internationally, we focused our current investigation on this specific lineage.

PJ.2.1 harbors multiple substitutions within the receptor-binding domain (RBD) on sites previously frequently observed mutating, including R346T, N439K, K440N, 445P, 452K, and S446T. These substitutions, thoroughly documented in prior deep mutational scanning and experimental studies, are known to modulate ACE2 binding affinity and mediate antibody escape [3-5]. Additionally, PJ.2.1 has acquired more than 10 mutations across the SD1, 630-loop region, S1/S2 cleavage sites, and S2 subunit domain. This extensive mutational profile indicates a high probability of significant alterations in the structural configuration of the spike protein. To assess whether PJ.2.1 possesses virological and antigenic characteristics associated with a potential transmission advantage, we compared it with its ancestral strain, MC.10.1 (a sublineage of KP.3.1.1), as well as the currently circulating variants NB.1.8.1, PQ.16.1.1, BA.3.2.2, and XFG [6-8].

We first generated spike-pseudotyped vesicular stomatitis viruses bearing the spike proteins of

PJ.2.1_ON, MC.10.1, KP.3.1.1, NB.1.8.1, PQ.16.1.1, and XFG, assessing their receptor engagement capability via susceptibility to inhibition by soluble human angiotensin-converting enzyme 2 (hACE2). PJ.2.1_ON exhibited an hACE2 inhibition IC50 comparable to that of KP.3.1.1 and slightly lower than that of MC.10.1. Crucially, its IC50 was substantially lower than those of the contemporary circulating variants NB.1.8.1, PQ.16.1.1, and XFG (Figure 1C). Because a lower hACE2 inhibition IC_{50} indicates more efficient interaction with soluble hACE2, these findings suggest that PJ.2.1_ON has a higher hACE2-binding affinity and more efficient receptor engagement than contemporary lineages.

Next, we generated stabilized spike trimers (S6P) corresponding to NB.1.8.1, XFG, BA.3.2.2, and PJ.2.1_ON to quantify their binding affinities for soluble hACE2 utilizing surface plasmon resonance (SPR). Among the tested variants, PJ.2.1_ON exhibited the highest hACE2-binding affinity, followed by NB.1.8.1, XFG, and BA.3.2.2. These results are consistent with the hACE2 inhibition assay, directly indicating the superior hACE2 engagement by PJ.2.1_ON compared to the other tested variants (Figure 1D and S1). Collectively, these findings suggest the unique set of mutations in PJ.2.1_ON enhances the spike-ACE2 interaction, potentially facilitating more efficient cellular entry. This enhanced receptor engagement is likely driven not solely by RBD mutations, but also by NTD, 630-loop, and S1/S2 cleavage site substitutions, which exert allosteric effects that may alter the RBD “up” and “down” conformational dynamics.

We also evaluated the antigenic properties and humoral immune evasion profiles of these variants using pseudovirus neutralization assays. Antigenicity was mapped using sera from naive mice immunized twice with spike-encoding mRNA vaccines, while humoral immune evasion was evaluated using recent plasma sourced from humans with varying exposure histories. Antigenic cartography based on mice sera revealed that PJ.2.1 surprisingly clustered closely with members of the currently circulating JN.1 family, indicating relatively short antigenic distances (Figure 1E). In plasma from Omicron-primed individuals (defined as unvaccinated cohorts with a primary Omicron infection history), the neutralization sensitivity of PJ.2.1_ON was comparable to MC.10.1, KP.3.1.1, NB.1.8.1, and XFG, with no statistically significant differences in neutralization titers (Figure 1F). In contrast, in plasma from individuals primed with inactivated Wuhan-Hu-1 vaccines, neutralization titers against PJ.2.1_ON were even significantly higher than those against the other

variants tested, including MC.10.1 (Figure 1F). These results confirm that PJ.2.1_ON remains antigenically similar to circulating JN.1-family variants, has not developed substantial humoral immune evasion capabilities, and may even display increased susceptibility to antibody neutralization.

We further extended our immunological profiling utilizing a comprehensive panel of RBD-targeting neutralizing monoclonal antibodies (mAbs) representing distinct epitope classes [4-5]. Compared to MC.10.1, PJ.2.1_ON did not exhibit increased evasion against class 1 and class 1/4 antibodies (Figure 1G). This contrasts with XFG and PQ.16.1.1, which demonstrated substantially greater immune evasion against class 1 mAbs, and BA.3.2.2, which exhibited marked evasion against class 1/4 mAbs relative to PJ.2.1_ON. However, likely due to multiple mutations within the 439–450 loop, PJ.2.1_ON demonstrated a BA.3.2.2-like enhanced resistance to class 3 antibodies. Notably, these class 3 antibodies are largely Omicron-specific and are predominantly elicited in Omicron-primed individuals or through Omicron-induced de novo antibody responses [9].

Most importantly, PJ.2.1_ON displayed increased neutralization sensitivity compared to the other tested variants when exposed to class 4 and class 5 antibodies (Figure 1G). These mAbs target cryptic sites on the RBD that remain sterically inaccessible within a fully closed (3-down) spike trimer conformation. This contrast is especially pronounced when comparing PJ.2.1_ON with BA.3.2.2; the latter predominantly adopts an enriched 3-down RBD structural configuration and consequently showed minimal neutralization by cryptic-site-targeting mAbs [10]. The heightened neutralization sensitivity of PJ.2.1_ON—observed not only against cryptic-site targeting mAbs but also against class 1 mAbs, class 1/4 mAbs, and human plasma—strongly suggests an altered RBD conformational dynamic that favors the receptor-accessible “up” state, thereby exposing the internal epitopes targeted by class 4 and class 5 antibodies and improving accessibility for “up” RBD-targeting neutralization mAbs.

Taken together, we found that while PJ.2.1 lacks the extreme immune evasion capabilities of past wave drivers, it possesses a significantly higher human ACE2 binding affinity than currently dominant variants. This distinct phenotypic profile suggests PJ.2.1 may follow an evolutionary trajectory analogous to BA.2.86/JN.1. BA.2.86 similarly leveraged a high-affinity structural

foundation to subsequently acquire the L455S mutation, ultimately evolving into the highly evasive JN.1 variant that drove widespread global infections in 2024. Their robust ACE2 binding provides a structural buffer, enabling the rapid acquisition of strong immune-evasive mutations at the expense of binding affinity. Although current findings do not definitively establish an immediate transmission advantage, the global reporting of PJ.2.1 highlights the critical risk of further adaptation. The potential acquisition of known immune evasion-enhancing substitutions—such as A475V, N487D, and D420N, which are frequently observed in recent variants—could immediately enable PJ.2.1 descendants to reshape the epidemiological landscape. Consequently, continued genomic, epidemiological, and virological surveillance of PJ.2.1 is essential.

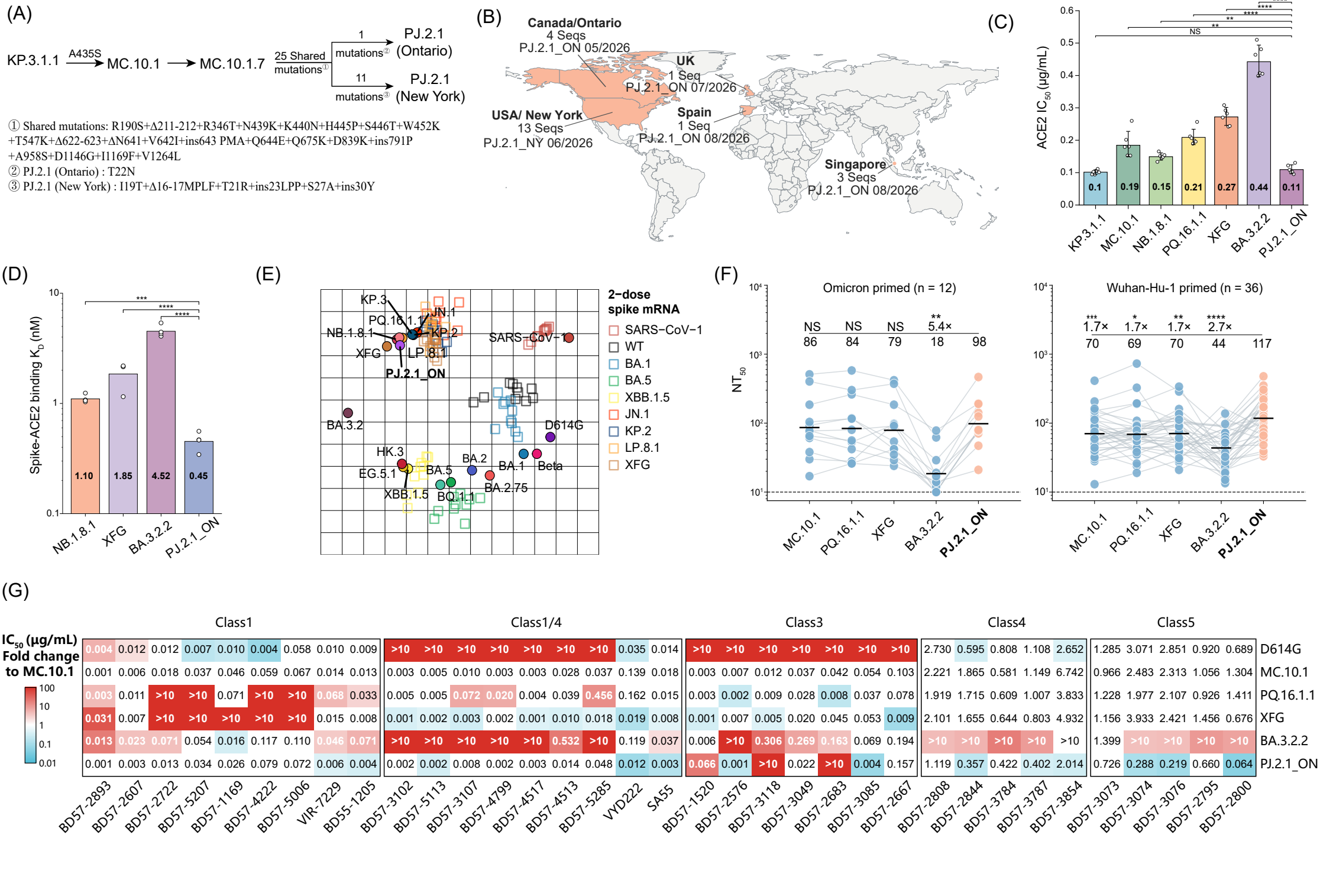
(A)
KP.3.1.1
A435S
MC.10.1
MC.10.1.7
25 Shared mutations①
1 mutations②
PJ.2.1 (Ontario)
11 mutations③
PJ.2.1 (New York)
① Shared mutations: R190S+Δ211-212+R346T+N439K+K440N+H445P+S446T+W452K +T547K+Δ622-623+ΔN641+V642I+ins643 PMA+Q644E+Q675K+D839K+ins791P +A958S+D1146G+I1169F+V1264L
② PJ.2.1 (Ontario) : T22N
③ PJ.2.1 (New York) : I19T+Δ16-17MPLF+T21R+ins23LPP+S27A+ins30Y
(B)
Canada/Ontario
4 Seqs
PJ.2.1_ON 05/2026
UK
1 Seq
PJ.2.1_ON 07/2026
USA/ New York
13 Seqs
PJ.2.1_NY 06/2026
Spain
1 Seq
PJ.2.1_ON 08/2026
Singapore
3 Seqs
PJ.2.1_ON 08/2026
(C)
ACE2 IC50 (μg/mL)
0.1
0.19
0.15
0.21
0.27
0.44
0.11
KP.3.1.1
MC.10.1
NB.1.8.1
PQ.16.1.1
XFG
BA.3.2.2
PJ.2.1_ON
(D)
Spike-ACE2 binding KD (nM)
1.10
1.85
4.52
0.45
NB.1.8.1
XFG
BA.3.2.2
PJ.2.1_ON
(E)
KP.3
JN.1
PQ.16.1.1
NB.1.8.1
KP.2
XFG
LP.8.1
PJ.2.1_ON
SARS-CoV-1
BA.3.2
D614G
HK.3
BA.2
BA.1
Beta
EG.5.1
BA.5
BA.2.75
XBB.1.5
BQ.1.1
2-dose spike mRNA
SARS-CoV-1
WT
BA.1
BA.5
XBB.1.5
JN.1
KP.2
LP.8.1
XFG
(F)
Omicron primed (n = 12)
NT50
NS 86
NS 84
NS 79
5.4× 18
98
MC.10.1
PQ.16.1.1
XFG
BA.3.2.2
PJ.2.1_ON
Wuhan-Hu-1 primed (n = 36)
1.7× 70
1.7× 69
1.7× 70
2.7× 44
117
MC.10.1
PQ.16.1.1
XFG
BA.3.2.2
PJ.2.1_ON
(G)
IC50 (μg/mL) Fold change to MC.10.1
100
10
1
0.1
0.01
Class1
Class1/4
Class3
Class4
Class5
D614G
MC.10.1
PQ.16.1.1
XFG
BA.3.2.2
PJ.2.1_ON
BD57-2893
BD57-2607
BD57-2722
BD57-5207
BD57-1169
BD57-4222
BD57-5006
VIR-7229
BD55-1205
BD57-3102
BD57-5113
BD57-3107
BD57-4799
BD57-4517
BD57-4513
BD57-5285
VYD222
SA55
BD57-1520
BD57-2576
BD57-3118
BD57-3049
BD57-2683
BD57-3085
BD57-2667
BD57-2808
BD57-2844
BD57-3784
BD57-3787
BD57-3854
BD57-3073
BD57-3074
BD57-3076
BD57-2795
BD57-2800

Figure Legends

Figure 1 | Virological, epidemiological, and antigenic characterization of the the SARS-CoV-2 saltation variant PJ.2.1

(A) Schematic evolutionary pathway and spike glycoprotein mutational profile of SARS-CoV-2 saltation variant PJ.2.1. PJ.2.1 (Ontario) and PJ.2.1 (New York) represent distinct clinical isolates.

(B) Global geographic distribution of SARS-CoV-2 variant PJ.2.1. Coral shading highlights countries with detected cases. Labels indicate geographic location, sequence counts, corresponding isolate (PJ.2.1_ON or PJ.2.1_NY), and earliest collection dates (month/year), using data retrieved from GISAID and NCBI GenBank.

(C) Soluble human ACE2 neutralization against KP.3.1.1, MC.10.1, NB.1.8.1, PQ.16.1.1, XFG, BA.3.2.2, and PJ.2.1_ON pseudoviruses. Columns and numeric values indicate geometric mean half-maximal inhibitory concentration (IC_{50}, μg/mL) values, with scatter points representing independent technical replicates. Statistical significance was evaluated using a two-tailed t test on log-transformed IC_{50} values.

(D) Surface plasmon resonance (SPR) measurement of human ACE2 (hACE2) binding affinities for NB.1.8.1, XFG, BA.3.2.2, and PJ.2.1_ON spike trimers. Bar heights and embedded values indicate geometric mean dissociation constants (K_D, nM) , with scatter points denoting individual technical replicates. Statistical significance was evaluated using two-tailed t test on log-transformed K_D values.

(E) Antigenic cartography based on serum NT50 titers from mice immunized with two doses of spike mRNA vaccines against indicated variants.

(F) Plasma neutralization titers against MC.10.1, PQ.16.1.1, XFG, BA.3.2.2, and PJ.2.1_ON pseudoviruses in Omicron-primed (n=12) and Wuhan-Hu-1-primed (n=36) cohorts. Solid horizontal lines and numerical values designate geometric mean titers (NT_{50}), with individual connected dots indicating paired plasma samples. The horizontal dashed line marks the limit of detection (NT_{50}=10). Statistical comparisons, fold changes relative to PJ.2.1_ON, and significance levels assessed by the

Wilcoxon rank-sum test are annotated above each variant.

(G) Neutralization profiles of RBD-directed monoclonal antibodies across distinct epitope classes against indicated SARS-CoV-2 pseudoviruses. Background color gradient depicts fold changes relative to MC.10.1, where red indicates increased resistance and blue denotes heightened sensitivity according to the color scale. IC_{50}=50% inhibitory concentration. NS=not significant. NT_{50}=50% neutralisation titre. *p<0.05. **p<0.01. ***p<0.001. ****p<0.0001.

Declaration of interests

Y.C. has provisional patent applications for the BD series antibodies (WO2024131775A9 and WO2023151312A1) and is the founder of Singlomics Biopharmaceuticals. All other authors declare no competing interests.

References

1. Yang S, Yu Y, Jian F et al. Antigenicity and infectivity characterisation of SARS-CoV-2 BA.2.86. The Lancet Infectious Diseases, 2023; 23, e457-e459

2. Yang, S., Yu, Y., Xu, Y. et al. Fast evolution of SARS-CoV-2 BA.2.86 to JN.1 under heavy immune pressure. The Lancet Infectious Diseases. 2023; 24:e70–e72.

3. Starr, T.N., Greaney, A.J., Hilton, S.K. et al. Deep Mutational Scanning of SARS-CoV-2 Receptor Binding Domain Reveals Constraints on Folding and ACE2 Binding. Cell. 2020; 182:1295-1310.e20.

4. Jian, F., Wang, J., Yisimayi, A. et al. Evolving antibody response to SARS-CoV-2 antigenic shift from XBB to JN.1. Nature. 2025; 637:921–929.

5. Yisimayi, A., Song, W., Wang, J. et al. Repeated Omicron exposures override ancestral SARS-CoV-2 immune imprinting. Nature. 2024; 625:148-156.

6. Liu J, Yu Y, Jian F et al. Enhanced immune evasion of SARS-CoV-2 variants KP.3.1.1 and XEC through N-terminal domain mutations. The Lancet Infectious Diseases, 2024; 25, e6-e7

7. Guo C, Yu Y, Liu J et al. Antigenic and virological characteristics of SARS-CoV-2 variants BA.3.2, XFG, and NB.1.8.1. The Lancet Infectious Diseases, 2025; 25, e374-e377

8. He P, Song Y, Guo C et al. Antibody evasion and receptor binding of SARS-CoV-2 variants PQ.16.1.1 and RK.1. The Lancet Infectious Diseases, 2026; 0

9. Johnston, T.S., Li, S.H., Painter, M.M. et al. Potent type-specific de novo antibodies complement broadly reactive imprinted antibodies in immune responses to SARS-CoV-2 variants. Nat Immunol 27, 1874–1886 (2026). https://doi.org/10.1038/s41590-026-02613-4

10. Stuart D, Dijokaite-Guraliuc A, Duyvesteyn H et al. Emerging SARS-CoV-2 variant BA.3.2 is more poorly neutralized by responses focused on other contemporary strains, 02 June 2026, Research Square [https://doi.org/10.21203/rs.3.rs-9585124/v1]

Appendix

Acknowledgments

We extend our gratitude to the scientific community for their continued efforts in monitoring SARS-CoV-2 variants, as well as to all volunteers who contributed blood samples for this study. This project is financially supported by Changping Laboratory (2026D-04-01 to Y.C.).

Author Contributions

Y.C. designed and supervised the study. P.H., B.L. and Y.C. wrote the manuscript with input from all authors. P.H., B.L. and C.G. performed the sequence analyses and prepared the illustrations. Y.Y. constructed the pseudoviruses. L.Y. and F.S. processed the plasma samples and performed the pseudovirus neutralisation assays. P.H. and Y.C. analysed the neutralisation data.

Methods Details

Genomic sequence analysis and lineage definition

SARS-CoV-2 sequence metadata for the saltation variant PJ.2.1 and related reference lineages evaluated in this study were retrieved from the GISAID EpiCoV[1] and NCBI GenBank databases on September 1, 2026. For the emerging saltation variant PJ.2.1, all available records collected from May to August 2026. Lineage assignments and aliases were verified according to the Pango nomenclature criteria outlined in lineage_notes.txt and alias_key.json from the cov-lineages/pango-designation repository. PJ.2.1 isolates identified from Ontario (Canada) and New York (USA) were referred to as PJ.2.1_ON and PJ.2.1_NY. These curated data were used to determine the geographic distribution, total sequence counts, and earliest collection dates across affected countries.

Surface Plasmon Resonance

Binding kinetics of SARS-CoV-2 spike trimers to human ACE2 were determined on a Biacore 8K instrument (Cytiva, cat. no. 12914229). Human ACE2 was captured onto Protein A sensor chips (Cytiva, cat. no. 29127556). Purified spike trimer ectodomains of the indicated variants were prepared in a twofold serial dilution series across six concentrations (ranging from 3.125 to 100 nM) and flowed across the chip surface in multi-cycle kinetics mode at ambient temperature. Sensorgrams were acquired with Biacore 8K Control Software (v.4.0.8.19879; Cytiva). Kinetic

association and dissociation rates as well as equilibrium dissociation constants (K_D) were obtained through global fitting to a 1:1 binding model using Biacore 8K Evaluation Software (v.4.0.8.20368; Cytiva).

Cohort recruitment and plasma processing

Peripheral blood samples were obtained from individuals enrolled in the study following the acquisition of written informed consent. Consent covered specimen procurement, biorepository storage, scientific investigation, and subsequent data dissemination. Study protocols received formal approval from the Tianjin Municipal Health Commission, the Institutional Review Board of Tianjin First Central Hospital (approval no. KEYAN20241022-2), and the Ethics Committee of Beijing Ditan Hospital, Capital Medical University (approval no. DTEC-KY2024-112-01). All procedures complied strictly with the ethical standards of the Declaration of Helsinki.For specimen isolation, whole blood was mixed 1:1 (v/v) with phosphate-buffered saline supplemented with 2% fetal bovine serum. Density-gradient centrifugation using Ficoll-Paque media (Cytiva, cat. no. 17-1440-03) was conducted to fractionate peripheral blood mononuclear cells and plasma. The cell-free plasma supernatant was harvested, divided into single-use aliquots, and cryopreserved at –20° C or lower. Prior to downstream neutralization assays, all plasma specimens were heat-inactivated at 56°C for 30 min.

Pseudovirus neutralization assay

SARS-CoV-2 spike pseudoviruses were produced using a vesicular stomatitis virus (VSV)-based packaging system. Briefly, 293T cells (ATCC, CRL-3216) were transfected with spike-expression plasmids together with G*ΔG-VSV (Kerafast). Culture supernatants were harvested, filtered, aliquoted, and stored at −80°C.For neutralization assays, pseudoviruses were incubated with serially diluted monoclonal anti-S-RBD antibodies, human ACE2-Fc, or heat-inactivated plasma in 96-well plates at 37°C with 5% CO_2 for 1 h. Plasma samples were initially diluted 1:10, followed by five consecutive threefold dilutions. Monoclonal antibodies and human ACE2-Fc (initial concentration 0.1 mg/mL) were pre-diluted 1:100 and 1:50, respectively, followed by five consecutive fivefold dilutions. Huh-7 cells (JCRB, 0403) were then added to each well. After 24 h of incubation, supernatants were removed and D-luciferin reagent (Vazyme, DD1209-03) was added. Luminescence was measured using a microplate spectrophotometer (PerkinElmer, HH3400) after 2

min in the dark. Half-maximal inhibitory concentration (IC_{50}) and NT_{50} values were calculated using a four-parameter logistic regression model.

Supplementary Tables

Table S1 | Spike protein sequences of SARS-CoV-2 variants

KP.3.1.1

MFVFLVLLPLVSSQCVMPLFNLITTTQSYTNFTRGVYYPDKVFRSSVLHLTQDLFLPFFSNVTWFHAISGTNGTKRFDNP
VLPFNDGVYFASTEKSNIIRGWIFGTTLDSKTQSLLIVNNATNVFIKVCEFQFCNDPFLDVYHKNNKSWMESESGVYSSA
NNCTFEYVSQPFLMDLEGKQGNFKNLREFVFKNIDGYFKIYSKHTPIIGRDFPQGFSALEPLVDLPIGINITRFQTLLALNRS
YLTPGDSSSGWTAGAADYYVGYLQPRTFLLKYNENGTITDAVDCALDPLSETKCTLKSFTVEKGIYQTSNFRVQPTESIVR
FPNVTNLCPFHEVFNATRFASVYAWNRTRISNCVADYSVLYNFAPFFAFKCYGVSPTKLNDLCFTNVYADSFVIKGNEV
SQIAPGQTGNIADYNYKLPDDFTGCVIAWNSNKLDSKHSGNYDYWYRSLRKSKLKPFERDISTEIYQAGNKPCKGKGPN
CYFPLESYGFRPTYGVGHQPYRVVVLSFELLHAPATVCGPKKSTNLVKNKCVNFNFNGLTGTGVLTKSNKKFLPFQQFG
RDIVDTTDAVRDPQTLEILDITPCSFGGVSVITPGTNTSNQVAVLYQGVNCTEVSVAIHADQLTPTWRVYSTGSNVFQT
RAGCLIGAEYVNNSYECDIPIGAGICASYQTQTKSRRRARSVASQSIIAYTMSLGAENSVAYSNNSIAIPTNFTISVTTEILP
VSMTKTSVDCTMYICGDSTECSNLLLQYGSFCTQLKRALTGIAVEQDKNTQEVFAQVKQIYKTPPIKYFGGFNFSQILPD
PSKPSKRSFIEDLLFNKVTLADAGFIKQYGDCLGDIAARDLICAQKFNGLTVLPPLLTDEMIAQYTSALLAGTITSGWTFGA
GAALQIPFAMQMAYRFNGIGVTQNVLYENQKLIANQFNSAIGKIQDSLFSTASALGKLQDVVNHNAQALNTLVKQLS
SKFGAISSVLNDILSRLDKVEAEVQIDRLITGRLQSLQTYVTQQLIRAAEIRASANLAATKMSECVLGQSKRVDFCGKGYH
LMSFPQSAPHGVVFLHVTYVPAQEKNFTTAPAICHDGKAHFPREGVFVSNGTHWFLTQRNFYEPQIITTDNTFVSGNC
DVVIGIVNNTVYDPLQPELDSFKEELDKYFKNHTSPDVDLGDISGINASVVNIQKEIDRLNEVAKNLNESLIDLQELGKYE
QYIKWPWYIWLGFIAGLIAIVMVTIMLCCMTSCCSCLKGCCSCGSCCKFDEDDSEPVLKGVKLHYT

MC.10.1

MFVFLVLLPLVSSQCVMPLFNLITTTQSYTNFTRGVYYPDKVFRSSVLHLTQDLFLPFFSNVTWFHAISGTNGTKRFDNP
VLPFNDGVYFASTEKSNIIRGWIFGTTLDSKTQSLLIVNNATNVFIKVCEFQFCNDPFLDVYHKNNKSWMESESGVYSSA
NNCTFEYVSQPFLMDLEGKQGNFKNLREFVFKNIDGYFKIYSKHTPIIGRDFPQGFSALEPLVDLPIGINITRFQTLLALNRS
YLTPGDSSSGWTAGAADYYVGYLQPRTFLLKYNENGTITDAVDCALDPLSETKCTLKSFTVEKGIYQTSNFRVQPTESIVR
FPNVTNLCPFHEVFNATRFASVYAWNRTRISNCVADYSVLYNFAPFFAFKCYGVSPTKLNDLCFTNVYADSFVIKGNEV
SQIAPGQTGNIADYNYKLPDDFTGCVISWNSNKLDSKHSGNYDYWYRSLRKSKLKPFERDISTEIYQAGNKPCKGKGPN
CYFPLESYGFRPTYGVGHQPYRVVVLSFELLHAPATVCGPKKSTNLVKNKCVNFNFNGLTGTGVLTKSNKKFLPFQQFG
RDIVDTTDAVRDPQTLEILDITPCSFGGVSVITPGTNTSNQVAVLYQGVNCTEVSVAIHADQLTPTWRVYSTGSNVFQT
RAGCLIGAEYVNNSYECDIPIGAGICASYQTQTKSRRRARSVASQSIIAYTMSLGAENSVAYSNNSIAIPTNFTISVTTEILP
VSMTKTSVDCTMYICGDSTECSNLLLQYGSFCTQLKRALTGIAVEQDKNTQEVFAQVKQIYKTPPIKYFGGFNFSQILPD
PSKPSKRSFIEDLLFNKVTLADAGFIKQYGDCLGDIAARDLICAQKFNGLTVLPPLLTDEMIAQYTSALLAGTITSGWTFGA
GAALQIPFAMQMAYRFNGIGVTQNVLYENQKLIANQFNSAIGKIQDSLFSTASALGKLQDVVNHNAQALNTLVKQLS
SKFGAISSVLNDILSRLDKVEAEVQIDRLITGRLQSLQTYVTQQLIRAAEIRASANLAATKMSECVLGQSKRVDFCGKGYH
LMSFPQSAPHGVVFLHVTYVPAQEKNFTTAPAICHDGKAHFPREGVFVSNGTHWFLTQRNFYEPQIITTDNTFVSGNC
DVVIGIVNNTVYDPLQPELDSFKEELDKYFKNHTSPDVDLGDISGINASVVNIQKEIDRLNEVAKNLNESLIDLQELGKYE
QYIKWPWYIWLGFIAGLIAIVMVTIMLCCMTSCCSCLKGCCSCGSCCKFDEDDSEPVLKGVKLHYT

NB.1.8.1

MFVFLVLLPLVSSQCVMPLFNLITTNQSYTNSFTRGVYYPDKVFRSSVLHLTQDLFLPFSSNVTWFHAISGTNGTKRFDN
PVLPFNDGVYFASTEKSNIIRGWIFGTTLDSKTQSLLIVNNATNVFIKVCEFQFCNDPFLDVYHKNNKSWMESESGVYSS
ANNCTFEYVSQPFLMDLEGKQSNFKNLREFVFKNIDGYFKIYSKHTPIIGRDFPQGFSALEPLVDLPIGINITRFQTLLALNR
SYLTPGDSSSGWTAGAADYYVGYLQPRTFLLKYNENGTITDAVDCALDPLSETKCTLKSFTVEKGIYQTSNFRVQPTESIV

RFPNVTNLCPFHEVFNATRFASVYAWNRTRISNCVADYSVLYNFAPFFAFKCYGVSPTKLNDLCFTNVYADSFVIKGNE
VSQIAPGQTGNIADYNYKLPDDFTGCVISWNSNKLDSKHSGNYDYWYRSLRKSKLKPFERDISTEIYQAGNIPCKGKGP
NCYFPLESYGFRPTYGVGHQPYRVVVLSFELLHAPATVCGPKKSTNLVKNKCVNFNFNGLTGTGVLTKSNKKFLPFQQF
GRDIVDTTDAVRDPQTLEILDITPCSFGGVSVITPGTNTSNQVAVLYQGVNCTEVSVAIHADQLTPTWRVYSTGSNVFQ
TRAGCLIGAEYVNNSYECDIPIGAGICASYQTQTKSRRRARSVASQSIIAYTMSLGAENSVAYSNNSIAIPTNFTISVTTEIL
PVSMTKTSVDCTMYICGDSTECSNLLLQYGSFCTQLKRALTGIAVEQDKNTQEVFAQVKQIYKTPPIKYFGGFNFSQILP
DPSKPSKRSFIEDLLFNKVTLADAGFIKQYGDCLGDIAARDLICAQKFNGLTVLPPLLTDEMIAQYTSALLAGTITSGWTFG
AGAALQIPFAMQMAYRFNGIGVTQNVLYENQKLIANQFNSAIGKIQDSLFSTASALGKLQDVVNHNAQALNTLVKQL
SSKFGAISSVLNDILSRLDKVEAEVQIDRLITGRLQSLQTYVTQQLIRAAEIRASANLAATKMSECVLGQSKRVDFCGKGY
HLMSFPQSAPHGVVFLHVTYVPAQEKNFTTAPAICHDGKAHFPREGVFVSNGTHWFVTQRNFYEPQIITTDNTFVSGN
CDVVIGIVNNTVYDPLQLELDSFKEELDKYFKNHTSPDVDLGDISGINASVVNIQKEIDRLNEVAKNLNESLIDLQELGKYE
QYIKWPWYIWLGFIAGLIAIVMVTIMLCCMTSCCSCLKGCCSCGSCCKFDEDDSEPVLKGVKLHYT

PQ.16.1.1

MFVFLVLLPLVSSQCVMPLFNLITTNQSYTNSFTRGVYYPDKVFRSSVLHLTQDLFLPFSSNVTWFHAISGTNGTKRFDN
PVLPFNDGVYFASTEKSNIIRGWIFGTTLDSKTQSLLIVNNATNVFIKVCEFQFCNDPFLDVYHKNNKSWMESESGVYSS
ANNCTFEYVSQPFLMDLEGKQSNFKNLREFVFKNIDGYFKIYSKHTPIIGRDFPQGFSALEPLVDLPIGINITRFQTLLALNR
SYLTPGGSSSGWTAGAADYYVGYLQPRTFLLKYNENGTITDAVDCALDPLSETKCTLKSFTVEKGIYQTSNFRVQPTESIV
RFPNVTNLCPFHEVFNATRFASVYAWNRTRISNCVADYSVLYNFAPFFAFKCYGVSPTKLNDLCFTNVYADSFVIKGNE
VSQIAPGQTGTIANYNYKLPDDFTGCVISWNSNKLDSKHSGNYDYWYRSLRKSKLKPFERDISTEIYQAGNTPCKGKGP
NCYFPLESYGFRPTYGVGHQPYRVVVLSFELLHAPATVCGPKKSTNLVKNKCVNFNFNGLTGTGVLTKSNKKFLPFQQF
GRDIVDTTDAVRDPQTLEILDITPCSFGGVSVITPGTNTSNQVAVLYQGVNCTEVSVAIHADQLTPTWRVYSTGSNVFQ
TRAGCLIGAEYVNNSYECDIPIGAGICASYQTQTKSRRRARSVASQSIIAYTMSLGAENSVAYSNNSIAIPTNFTISVTTEIL
PVSMTKTSVDCTMYICGDSTECSNLLLQYGSFCTQLKRALTGIAVEQDKNTQEVFAQVKQIYKTPPIKYFGGFNFSQILP
DPSKPSKRSFIEDLLFNKVTLADAGFIKQYGDCLGDIAARDLICAQKFNGLTVLPPLLTDEMIAQYTSALLAGTITSGWTFG
AGAALQIPFAMQMAYRFNGIGVTQNVLYENQKLIANQFNSAIGKLQDVVNHNAQALNTLVKQL
SSKFGAISSVLNDILSRLDKVEAEVQIDRLITGRLQSLQTYVTQQLIRAAEIRASANLAATKMSECVLGQSKRVDFCGKGY
HLMSFPQSAPHGVVFLHVTYVPAQEKNFTTAPAICHDGKAHFPREGVFVSNGTHWFVTQRNFYEPQIITTDNTFVSGN
CDVVIGIVNNTVYDPLQLELDSFKEELDKYFKNHTSPDVDLGDISGINASVVNIQKEIDRLNEVAKNLNESLIDLQELGKYE
QYIKWPWYIWLGFIAGLIAIVMVTIMLCCMTSCCSCLKGCCSCGSCCKFDEDDSEPVLKGVKLHYT

XFG

MFVFLVLLPLVSSQCVMPLFNLITTNQSYTNPFTRGVYYPDKVFRSSVLHLTQDLFLPFFSNVTWFHAISGTNGTKRFDN
PVLPFNDGVYFASTEKSNIIRGWIFGTTLDSKTQSLLIVNNATNVFIKVCEFQFCNDPFLDVYHKNNKSWMESESGVYSS
ANNCTFEYVSQPFLMDLEGRQGNFKNLSEFVFKNIDGYFKIYSKHTPIIGRDFPQGFSALEPLVDLPIGINITRFQTLLALNR
SYLTPGDSSSGWTAGAADYYVGYLQPRTFLLKYNENGTITDAVDCALDPLSETKCTLKSFTVEKGIYQTSNFRVQPTESIV
RFPNVTNLCPFHEVFNATTFASVYAWNRTRISNCVADYSVLYNFAPFFAFKCYGVSPTKLNDLCFTNVYADSFVIKGNE
VSQIAPGQTGNIADYNYKLPDDFTGCVIAWNSNKLDSRRSGNYDYWYRSLRKSKLKPFERDISTEIYQAGNKPCKGKGP
DCYFPLESYGFRPTYGVGHQPYRVVVLSFELLHAPATVCGPKKSTNLVKNKCVNFNFNGLTGTGVLTKSNKKFLPFQQF
GRDIVDITDAVRDPQTLEILDITPCSFGGVSVITPGTNTSNQVAVLYQGVNCTEVSVAIHADQLTPTWRVYSTGSNVFQT
RAGCLIGAEYVNNSYECDIPIGAGICASYQTQTKSRRRARSVASQSIIAYTMSLGAENSVAYSNNSIAIPTNFTISVTTEILP
VSMTKTSVDCTMYICGDSTECSNLLLQYGSFCTQLKRALTGIAVEQDKNTQEVFAQVKQIYKTPPIKYFGGFNFSQILPD
PSKPSKRSFIEDLLFNKVTLADAGFIKQYGDCLGDIAARDLICAQKFNGLTVLPPLLTDEMIAQYTSALLAGTITSGWTFGA
GAALQIPFAMQMAYRFNGIGVTQNVLYENQKLIANQFNSAIGKIQDSLFSTASALGKLQDVVNHNAQALNTLVKQLS
SKFGAISSVLNDILSRLDKVEAEVQIDRLITGRLQSLQTYVTQQLIRAAEIRASANLAATKMSECVLGQSKRVDFCGKGYH
LMSFPQSAPHGVVFLHVTYVPAQEKNFTTAPAICHDGKAHFPREGVFVSNGTHWFVTQRNFYEPQIITTDNTFVSGNC

DVVIGIVNNTVYDPLQLELDSFKEELDKYFKNHTSPDVDLGDISGINASVVNIQKEIDRLNEVAKNLNESLIDLQELGKYE
QYIKWPWYIWLGFIAGLIAIVMVTIMLCCMTSCCSCLKGCCSCGSCCKFDEDDSEPVLKGVKLHYT

BA.3.2.2

MFVFLVLLLLVSSQCVNLTTTTQLPLAYTNSFTRGVYYPDKVFRSSVLHSTQDLFLPFFSNVTWFHVISGTNGTKRFDNP
VLPFNDGVYFASIEKSNITRGWIFGTTLDSKTQSLLIVNNATNVVIKVCEFQFNNKSWMESESRVYSSAKNCTFEYVFQPF
LMDLEGKQGNFTNLREFVFKNIDGYFKIYSKHTPIIVRASDTDLPQGFSALEPLVDLPIGINITRFQTLLHRSYLTSGDSSSG
WTAGAAAYYVGYLQPRTFLLKYNENGTITDAVDCALDPLSETKCTLKSFTVEKGIYQTSNFRVQPTESVVRFPNITNLCPF
YEVFNATRFPSVYAWNRTRISNCVADYSVLYNFAPFFTFKCYGVSPTKLNDLCFTNVYADSFVIKGNEVSQIAPGQTGNI
ADYNYKLPDDFTGCVISWNSNRLDSKADGNYNYWYRLFRKSKLKPFERDISTEIYQAGNNPCNGVKGFNCYFPLQSYS
FRPTYGVGYQPYRVVVLSFELLHAPATVCGPKNSTNLVKNKCVNFNFNGLTGTGVLTDSNKKFLPFQQFGRDIADTTDS
VRDPQTLDILDITPCSFGGVSVITPGTNTSNQVAVLYQGVNCTEVPVAIRADQLTPTWRVYSTGSKGFQTRAGCLIGAK
YVNNSYECDIPIGAGICASYQTQTRSHRRARSVDSQSIIAYTMSLGAENLVAYSNNSIAIPTNFTISVTTEILPVSMTKTSV
DCTMYICGDSTECSNLLLQYGSFCTQLKRALTGIAVEQDKNTQEVFAQVKQIYKTPPITYFGGFNFSQILPDPSKPSKRSFI
EDLLFNKVTLADAGFIKQYGDCLGDIAARDLICKQKFNGLTVLPPLLTDEMIAQYTSALLAGTITSGWTFGAGAALQIPFA
MQMAYRFNGIGVTQNVLYENQKLIANQFNSAIGKIQDSLFSTASALGKLQDVVNHNAQALNTLVKQLSSKFGAISSVL
NDILSRLDKVEAEVQIDRLITGRLQSLQTYVTQQLIRAAEIRASANLAATKMSECVLGQSKRVDFCGKGYHLMSFPQSAP
HGVVFLHVTYVPAQEKNFTTAPAICHDGKAHFPREGVFVSNGTHWFVTQRNFYEPQIITTDNTFVSGNCDVVIGIVNN
TVYDPLQPELDSFKEELDKYFKNHTSPDVDLGDISGINASVVNIQKEIERLNEVAKNLNESLIDLQELGKYEQYIKWPWYI
WLGFIAGLIAIVMVTIMLCCMTSCCSCLKGCCSCGSCCKFDEDDSEPVLKGVKLHYT

PJ.2.1_ON

MFVFLVLLPLVSSQCVMPLFNLITTNQSYTNFTRGVYYPDKVFRSSVLHLTQDLFLPFFSNVTWFHAISGTNGTKRFDNP
VLPFNDGVYFASTEKSNIIRGWIFGTTLDSKTQSLLIVNNATNVFIKVCEFQFCNDPFLDVYHKNNKSWMESESGVYSSA
NNCTFEYVSQPFLMDLEGKQGNFKNLSEFVFKNIDGYFKIYSKHTPIGRDFPQGFSALEPLVDLPIGINITRFQTLLALNRS
YLTPGDSSSGWTAGAADYYVGYLQPRTFLLKYNENGTITDAVDCALDPLSETKCTLKSFTVEKGIYQTSNFRVQPTESIVR
FPNVTNLCPFHEVFNATTFASVYAWNRTRISNCVADYSVLYNFAPFFAFKCYGVSPTKLNDLCFTNVYADSFVIKGNEVS
QIAPGQTGNIADYNYKLPDDFTGCVISWNSKNLDSKPTGNYDYKYRSLRKSKLKPFERDISTEIYQAGNKPCKGKGPNCY
FPLESYGFRPTYGVGHQPYRVVVLSFELLHAPATVCGPKKSTNLVKNKCVNFNFNGLKGTGVLTKSNKKFLPFQQFGRDI
VDTTDAVRDPQTLEILDITPCSFGGVSVITPGTNTSNQVAVLYQGVNCTEVSIHADQLTPTWRVYSTGSIFPMAETRAG
CLIGAEYVNNSYECDIPIGAGICASYKTQTKSRRRARSVASQSIIAYTMSLGAENSVAYSNNSIAIPTNFTISVTTEILPVSMT
KTSVDCTMYICGDSTECSNLLLQYGSFCTQLKRALTGIAVEQDKNTQEVFAQVKQIYKTPPPIKYFGGFNFSQILPDPSKP
SKRSFIEDLLFNKVTLADAGFIKQYGKCLGDIAARDLICAQKFNGLTVLPPLLTDEMIAQYTSALLAGTITSGWTFGAGAAL
QIPFAMQMAYRFNGIGVTQNVLYENQKLIANQFNSAIGKIQDSLFSTASALGKLQDVVNHNAQSLNTLVKQLSSKFGA
ISSVLNDILSRLDKVEAEVQIDRLITGRLQSLQTYVTQQLIRAAEIRASANLAATKMSECVLGQSKRVDFCGKGYHLMSFP
QSAPHGVVFLHVTYVPAQEKNFTTAPAICHDGKAHFPREGVFVSNGTHWFLTQRNFYEPQIITTDNTFVSGNCDVVIGI
VNNTVYDPLQLELGSFKEELDKYFKNHTSPDVDLGDFSGINASVVNIQKEIDRLNEVAKNLNESLIDLQELGKYEQYIKW
PWYIWLGFIAGLIAIVMVTIMLCCMTSCCSCLKGCCSCGSCCKFDEDDSEPLLKGVKLHYT

Table S2 | Kinetic parameters of SARS-CoV-2 variant spike binding to hACE2 measured by SPR

Sample	$K_a(M^{-1}\ s^{-1})$	$K_d\ (s^{-1})$	$K_D(M)$
NB.1.8.1-Spike	1.11E+05	1.20E-04	1.08E-09
NB.1.8.1-Spike	1.07E+05	1.33E-04	1.24E-09
NB.1.8.1-Spike	1.12E+05	1.16E-04	1.03E-09
NB.1.8.1-Spike	1.07E+05	1.13E-04	1.06E-09
XFG-Spike	8.50E+04	1.84E-04	2.16E-09
XFG-Spike	8.64E+04	1.86E-04	2.15E-09
XFG-Spike	1.33E+05	1.53E-04	1.15E-09
XFG-Spike	7.92E+04	1.74E-04	2.19E-09
PJ.2.1_ON-Spike	2.88E+05	9.91E-05	3.44E-10
PJ.2.1_ON-Spike	1.81E+05	1.01E-04	5.59E-10
PJ.2.1_ON-Spike	1.96E+05	9.19E-05	4.68E-10
PJ.2.1_ON-Spike	1.96E+05	9.11E-05	4.66E-10
BA.3.2.2-Spike	4.54E+04	1.85E-04	4.08E-09
BA.3.2.2-Spike	4.22E+04	1.81E-04	4.29E-09
BA.3.2.2-Spike	4.02E+04	2.16E-04	5.38E-09
BA.3.2.2-Spike	4.35E+04	1.93E-04	4.44E-09

Table S3 | Information of recruited SARS-CoV-2 convalescent participants

Sample Type	Gender	Age	Wuhan-1 primed	Sampling time point	NT_{50}				
					MC.10.1	PQ.16.1.1	XFG	BA.3.2.2	PJ.2.1_ON
Omicron primed individuals	female	39	no	2025/4/9	510	580	419	62	466
Omicron primed individuals	female	47	no	2025/4/9	93	118	42	12	47
Omicron primed individuals	male	75	no	2025/5/14	30	28	98	15	76
Omicron primed individuals	female	38	no	2025/5/28	78	53	95	29	141
Omicron primed individuals	female	21	no	2025/6/26	104	116	54	19	71
Omicron primed individuals	female	42	no	2025/7/2	185	261	185	78	193
Omicron primed individuals	female	79	no	2025/7/16	77	80	91	10	77
Omicron primed individuals	male	51	no	2025/7/16	17	26	24	14	21
Omicron primed individuals	female	52	no	2025/7/24	38	26	42	10	81
Omicron primed individuals	female	42	no	2025/8/13	61	42	29	14	125
Omicron primed individuals	female	68	no	2025/8/13	402	301	372	17	190
Omicron primed individuals	female	43	no	2025/8/13	65	56	35	10	79
Wuhan-Hu-1 primed individual	female	28	yes	2025/4/9	80	86	78	60	101
Wuhan-Hu-1 primed individual	female	57	yes	2025/4/16	130	76	160	48	213
Wuhan-Hu-1 primed individual	female	55	yes	2025/4/16	65	55	134	57	108
Wuhan-Hu-1 primed individual	female	40	yes	2025/4/16	59	81	94	39	145
Wuhan-Hu-1 primed individual	female	45	yes	2025/4/16	146	108	105	89	477
Wuhan-Hu-1 primed individual	female	31	yes	2025/4/23	28	35	63	26	89
Wuhan-Hu-1 primed individual	female	25	yes	2025/4/17	47	63	58	45	68
Wuhan-Hu-1 primed individual	male	36	yes	2025/4/24	37	24	47	55	132
Wuhan-Hu-1 primed individual	male	28	yes	2025/4/24	48	91	27	20	33
Wuhan-Hu-1 primed individual	female	36	yes	2025/4/24	65	85	121	71	117
Wuhan-Hu-1 primed individual	female	56	yes	2025/4/24	38	56	102	21	104
Wuhan-Hu-1 primed individual	male	61	yes	2025/5/14	30	45	37	38	57
Wuhan-Hu-1 primed individual	female	39	yes	2025/5/14	412	730	287	85	351
Wuhan-Hu-1 primed individual	female	35	yes	2025/5/23	119	190	106	93	112
Wuhan-Hu-1 primed individual	female	31	yes	2025/5/15	32	67	36	28	36
Wuhan-Hu-1 primed individual	female	36	yes	2025/5/15	55	94	122	29	187
Wuhan-Hu-1 primed individual	male	27	yes	2025/5/15	49	59	52	79	156
Wuhan-Hu-1 primed individual	female	48	yes	2025/5/15	151	193	338	36	247
Wuhan-Hu-1 primed individual	female	75	yes	2025/5/28	206	326	43	174	84
Wuhan-Hu-1 primed individual	male	43	yes	2025/5/28	62	68	99	91	58
Wuhan-Hu-1 primed individual	female	31	yes	2025/6/26	40	46	78	28	39
Wuhan-Hu-1 primed individual	male	23	yes	2025/6/26	67	65	92	25	188
Wuhan-Hu-1 primed individual	female	69	yes	2025/7/2	109	88	136	39	242
Wuhan-Hu-1 primed individual	female	11	yes	2025/7/2	81	64	74	18	58
Wuhan-Hu-1 primed individual	female	18	yes	2025/7/4	162	91	90	29	173
Wuhan-Hu-1 primed individual	male	43	yes	2025/7/11	13	19	29	123	67
Wuhan-Hu-1 primed individual	male	20	yes	2025/7/18	92	54	58	35	128
Wuhan-Hu-1 primed individual	male	57	yes	2025/7/24	69	26	43	80	276
Wuhan-Hu-1 primed individual	female	54	yes	2025/8/1	98	62	39	17	118
Wuhan-Hu-1 primed individual	male	26	yes	2025/8/1	92	40	55	25	220
Wuhan-Hu-1 primed individual	female	28	yes	2025/8/8	44	44	46	24	74
Wuhan-Hu-1 primed individual	female	25	yes	2025/8/8	68	78	112	47	48
Wuhan-Hu-1 primed individual	female	23	yes	2025/8/8	89	43	31	73	169
Wuhan-Hu-1 primed individual	female	39	yes	2025/8/8	112	55	47	66	305
Wuhan-Hu-1 primed individual	female	48	yes	2025/8/26	75	38	21	41	171
Wuhan-Hu-1 primed individual	female	37	yes	2025/8/26	59	64	61	19	66

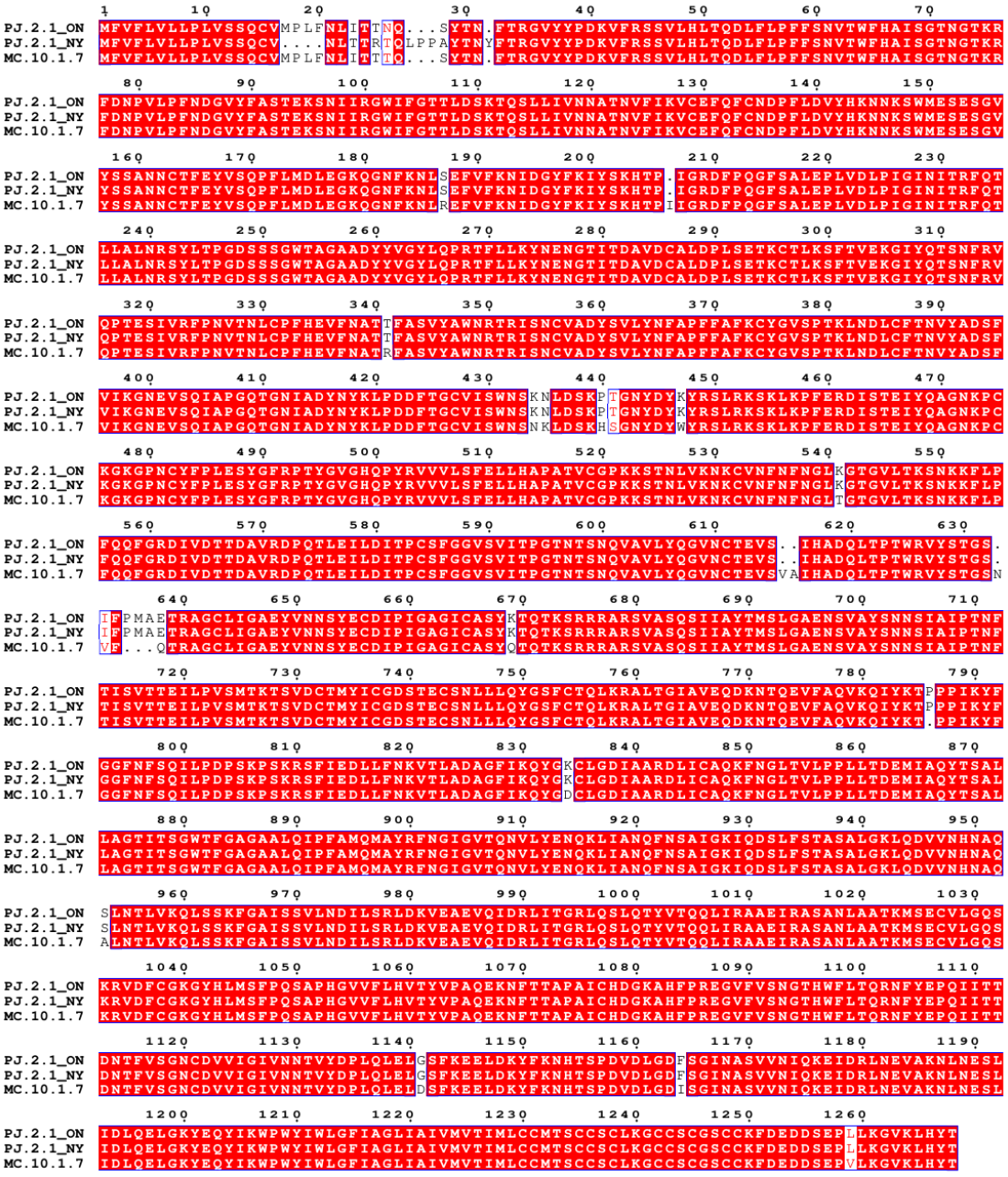

Figure S1 | Amino acid sequence alignment of Spike glycoproteins from SARS-CoV-2 varian t PJ.2.1 isolates and MC.10.1.7

Multiple sequence alignment of full-length spike proteins from representative PJ.2.1 isolates identified in Ontario, Canada (PJ.2.1_ON) and New York, USA (PJ.2.1_NY) alongside the reference lineage MC.10.1.7. Sequences were aligned using MAFFT and visualized with ESPript 3.2[2]. Identical residues are highlighted with red backgrounds and white text; blue frames denote residues with similar physicochemical properties; dots represent alignment gaps.

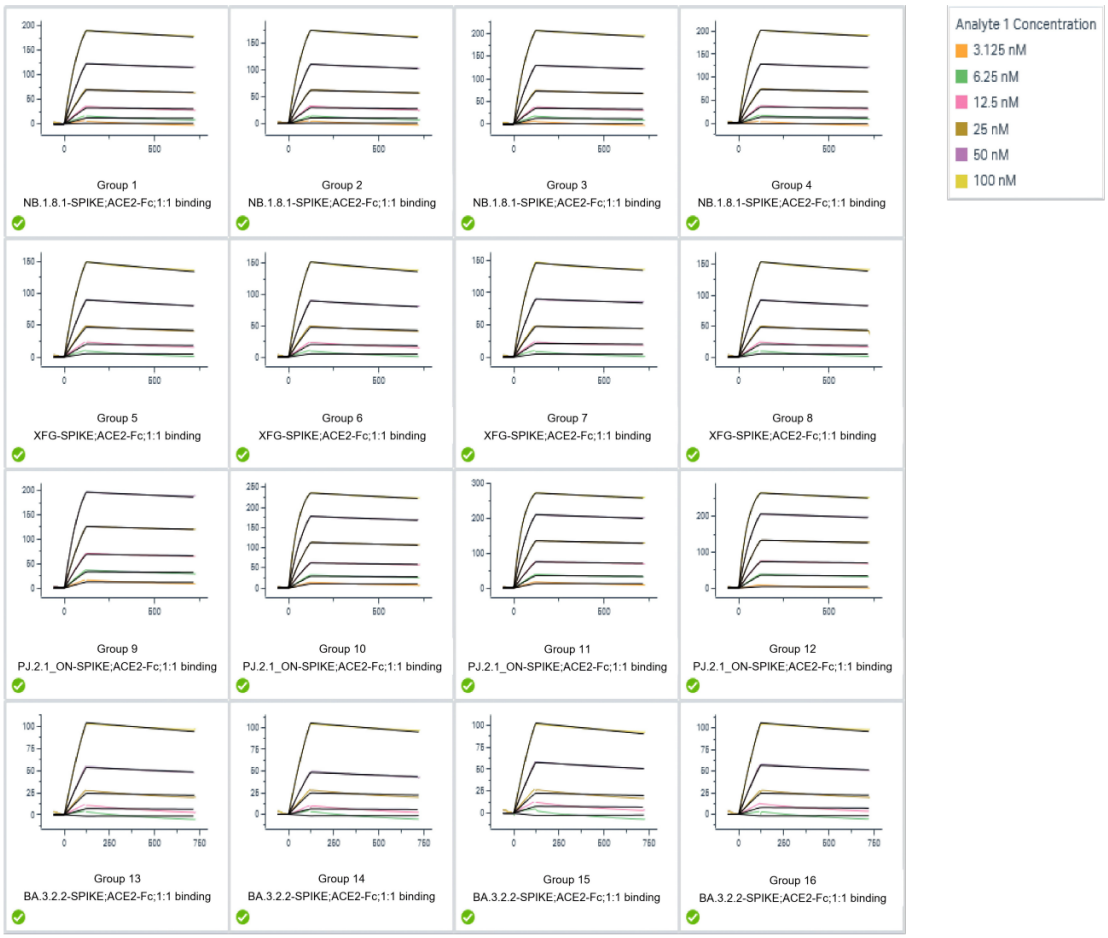

Figure S2 | Surface plasmon resonance (SPR) sensorgrams measuring binding kinetics of human ACE2 to SARS-CoV-2 variant spike trimers.

Kinetic profiles were acquired using multi-cycle kinetics runs on a Biacore 8K system. Twofold serial dilutions of purified SARS-CoV-2 spike glycoproteins were flowed over human ACE2 captured on Protein A sensor chips at room temperature. Raw binding responses are depicted as colored curves, overlaid with black lines denoting theoretical fits derived from a 1:1 binding model. Kinetic parameters, including association rate constant (ka), dissociation rate constant (kd), and equilibrium dissociation constant (K_D), were analyzed using Biacore 8K Evaluation Software (version 4.0.8.20368).

Supplementary References

1. Shu, Y ., John, M.C. GISAID: Global initiative on sharing all influenza data–from vision to reality. Euro Surveill. 2017; 22: 30494.

2. Gouet, P., Robert, X., Courcelle, E. ESPript/ENDscript: extracting and rendering sequence and 3D information from atomic structures of proteins. Nucl. Acids Res. 2003; 31: 3320-3323.